Song *et al. J. Mater. Inf.* **2025**, *5*, 2
DOI: 10.20517/jmi.2024.70

Journal of Materials Informatics

Research Article

Open Access

Predicting stacking fault energy in austenitic stainless steels via physical metallurgy-based machine learning approaches

Longyu Song, Chenchong Wang, Yizhuang Li, Xiaolu Wei*

State Key Laboratory of Rolling and Automation, Northeastern University, Shenyang 110819, Liaoning, China.

***Correspondence to:** Dr. Xiaolu Wei, State Key Laboratory of Rolling and Automation, Northeastern University, NO. 3-11, Wenhua Road, Heping District, Shenyang 110819, Liaoning, China. E-mail: weixl@smm.neu.edu.cn

How to cite this article: Song, L.; Wang, C.; Li, Y.; Wei, X. Predicting stacking fault energy in austenitic stainless steels via physical metallurgy-based machine learning approaches. *J. Mater. Inf.* **2025**, *5*, 2. https://dx.doi.org/10.20517/jmi.2024.70

Received: 9 Nov 2024 **First Decision:** 30 Nov 2024 **Revised:** 13 Dec 2024 **Accepted:** 23 Dec 2024 **Published:** 8 Jan 2025

Academic Editor: Xiaoyan Song **Copy Editor:** Pei-Yun Wang **Production Editor:** Pei-Yun Wang

Abstract

Stacking fault energy (SFE) significantly influences plastic deformation, strength, and processing performance, making accurate assessment and prediction of SFE essential for material design and optimization. Traditional SFE calculations mainly rely on experimental measurements and thermodynamic theories, with the former usually being time-consuming and the latter limited in applicability at different compositions. To overcome these limitations, this study proposes a machine learning (ML) strategy introducing physical metallurgy (PM) parameters relevant to SFE, aiming to achieve robust predictions. Specifically, this study evaluates three methods for introducing PM information into ML (as an input, an intermediate parameter, and a transfer source), with transfer learning as the best strategy. Initially, various PM parameters were calculated based on alloy composition and temperature, and subsequently used as outputs to train a convolutional neural network (CNN). This source model was then transferred to the SFE prediction model. The results from the model transfer using different PM information show that incorporating phase-transformation driving force (DF) as a source model for SFE prediction provided the most accurate and reliable results. This approach of introducing PM parameters into ML significantly improves the predictive capability of SFE models, offering a new perspective and solution for the prediction of SFE. Furthermore, this method may also be applicable to the prediction of other material properties during material design and optimization.

Keywords: Stacking fault energy, austenitic stainless steel, physical metallurgical parameter, machine learning, transfer learning

INTRODUCTION

Stacking fault energy (SFE) plays an important role in determining the susceptibility of a crystal to dislocation sliding and phase transformation during deformation. The outstanding mechanical properties of austenitic stainless steel, such as high plasticity and toughness, are partly attributed to its face-centered cubic (FCC) structure and relatively low SFE. Under specific conditions, a lower SFE facilitates deformation twinning and can induce a phase transformation from an FCC to a hexagonal close-packed (HCP) structure, enhancing the deformation mechanism, strength and processing performance of the alloy[1-4]. Therefore, accurate assessment and prediction of the SFE are essential for material design, as mastering SFE variations facilitates optimizing material microstructure, resulting in higher strength while maintaining plasticity and better addressing the need for high-performance materials in fields such as aerospace[5].

SFE calculation methods are categorized into experimental and theoretical approaches[6-10]. Experimental methods such as transmission electron microscopy (TEM), X-ray diffraction (XRD), and neutron diffraction (ND) directly measure stacking fault characteristics, which are then used to calculate the SFE. Whelan[11] established a theoretical foundation by examining extended dislocation nodes in steel grades; advancements in imaging techniques enabled researchers[12,13] to observe partial dislocation separations through weak-beam dark-field modes, a method widely applied in multi-component austenitic steels but limited to low SFE values. Reed and Schramm[14] determined the SFE using XRD line profile analysis, relating SFE to stacking fault probability, and rms microstrain. ND, similar to XRD but using thermal neutrons, also enables SFE determination. However, these experimental methods encounter a significant problem: the material constants in computational equations often derive from approximated values based on similar compositions, introducing uncertainties, and experimental measurement of the SFE is time-consuming and complex, hindering rapid material discovery. Given the dependence of SFE on alloy composition and temperature, empirical equations, thermodynamic models, and density functional theory (DFT) have emerged as alternative calculation methods. While several authors have developed empirical equations tailored to limited alloy compositions[15-17], their applicability is restricted. de Bellefon *et al.* collected 144 austenitic steel composition measurements and accurately predicted the SFE using linear regression[18]. As discussed in Supplementary Figure 1, Olson and Cohen[19] introduced a thermodynamic model conceptualizing stacking fault occurrence as an FCC-to-HCP transformation, calculating the change in energy per unit area, though its reliability depends heavily on the quality of the calculation of phase diagrams (CALPHAD) database[20-24]. The DFT suggested by Hohenberg and Kohn[25] calculates the SFE when the slip surface slides into a stable crystal structure by creating a crystal cell from an atomic perspective rather than depending on thermodynamic models or empirical equations. However, model building and optimization remain challenging and time-consuming.

The material genome initiative (MGI) has spurred data-driven, machine learning (ML)-based approaches[26,27] for SFE calculations. For example, Chaudhary *et al.* constructed a ML-based classifier for SFE prediction, facilitating the prediction of deformation mechanisms for unknown alloys[28]. Khan *et al.* proposed a framework combining DFT calculations, ML, and physical properties to predict SFE in entropy alloys[29]. Although these studies correlate alloy composition with SFE, predictive accuracy remains limited, and the ML model often lacks interpretability. Therefore, incorporating domain expertise [physical metallurgy (PM) parameters] into ML models to improve predictive accuracy and interpretability has become an important strategy, with promising results demonstrated[30-32]. For instance, Shen *et al.* incorporated thermodynamic methods on precipitated phases in ultra-high-strength stainless steels as ML model inputs for hardness prediction, achieving accurate, generalized predictions and optimizations in alloy design[33]. Basha *et al.* considered the role of fully connected layers in convolutional neural networks (CNNs) by analyzing layer-dataset feature relationships by changing their numbers, providing a novel approach for

the incorporation of PM information into deep learning models[34]. Wei *et al.* showed that using source features related to target performance aids in predictive transfer, highlighting effective incorporation of PM mechanisms into ML models[35]. Despite these advancements, ML-based SFE prediction models introducing PM knowledge remain underexplored.

In this study, we systematically compare different strategies for introducing PM information into ML, examining PM variables affecting SFE to obtain a generic prediction model. Using experimentally collected datasets on alloy composition, temperature, and SFE, we derived relevant PM data through thermodynamic calculations. Three PM introduction methods were explored: (i) direct input as features; (ii) inclusion in CNN fully connected layers; and (iii) transfer learning, where the source model predicting PM data transfers to the SFE prediction model. We evaluated the performance of each method and identified transfer learning as the optimal approach, providing methodological insights for universal SFE prediction and contributing to alloy design and development.

MATERIALS AND METHODS

Dataset and data preprocessing

Multiple publicly available SFE databases for austenitic alloys[28] were referenced and employed, containing experimental SFE measurements for several steel grades at different temperatures. Since the majority of data were measured at 300 K and SFE measurements at other temperatures are scarce and highly variable, only the SFE data recorded at 300 K were retained for this study. In addition, the original database was further screened to remove data with large errors, and the same compositions were averaged. This process resulted in a high-quality dataset of 188 samples containing 11-dimensional compositional features and SFE values, which were used for model training. To further refine the quality of the data, the phase transformation driving force (DF), and the Gibbs free energies of the FCC (G_{FCC}) and HCP (G_{HCP}) phases of the 188 sample alloys were computed using Thermo-Calc® software and the TCFE9 database. The details of the dataset are listed in Table 1. The distribution of the main elements and related PM parameters of the alloys in the dataset is shown in Figure 1, which contains compositional data for austenitic stainless steel, high-manganese steel, *etc.*

To ensure model stability and avoid the "lucky split" issue caused by random partitioning, this study rigorously divided the data into training and test sets at a ratio of 4:1, and repeated this random partitioning process 100 times to conduct a more in-depth analysis of the model's robustness. Additionally, for a comprehensive evaluation of each model's performance, we specifically selected 63 austenitic stainless steel SFE data[18] points as an independent validation set. This validation set is completely isolated from the training and test sets, with the aim of assessing the model's generalization capability in handling novel, unseen data.

This study also explores PM parameters of existing alloy systems to establish an extended dataset. Specifically, as shown in Figure 2A, 6,000 sets of new alloy samples were randomly generated within specified compositional ranges [chromium (Cr) < 25.85 wt.%; nickel (Ni) < 26.4 wt.%; manganese (Mn) < 27.5 wt.%; silicon (Si) < 6.22 wt.%]. All PM parameters for these samples, including DF, G_{FCC} and G_{HCP}, were calculated using Thermo-Calc®.

For data normalization, the inputs and outputs were normalized using the z-score, which is a standard method for eliminating dimensional differences between feature ranges[36], as determined by:

Table 1. Input and output ranges of the various parameters in the SFE database

Features	Minimum	Maximum	Mean	Standard deviation
Ferrum/wt.%	48.623	85	67.208	6.537
Cr/wt.%	0	25.85	15.23	5.777
Ni/wt.%	0	26.4	11.93	6.473
Mn/wt.%	0	27.5	4.35	7.106
Si/wt.%	0	6.22	0.41	1.12
Molybdenum/wt.%	0	2.7	0.64	1.06
Carbon/wt.%	0	0.69	0.054	0.124
Nitrogen/wt.%	0	0.88	0.059	0.135
Phosphorus/wt.%	0	0.08	0.009	0.015
Sulfur/wt.%	0	0.043	0.002	0.007
Aluminum/wt.%	0	3.98	0.11	0.551
DF/J·mol^{-1}	-1,663.99	1,892.676	-513.779	834.899
Gibbs free energy of the FCC phase/J·mol^{-1}	-18,546.5	-3,087.44	-6,174.99	3,186.666
Gibbs free energy of the HCP phase/J·mol^{-1}	-17,033.4	-3,823.53	-6,688.77	2,550.788
SFE/mJ·m^{-2}	3.26	70.15	35.3	13.7

SFE: Stacking fault energy; DF: driving force; FCC: face-centered cubic; HCP: hexagonal close-packed.

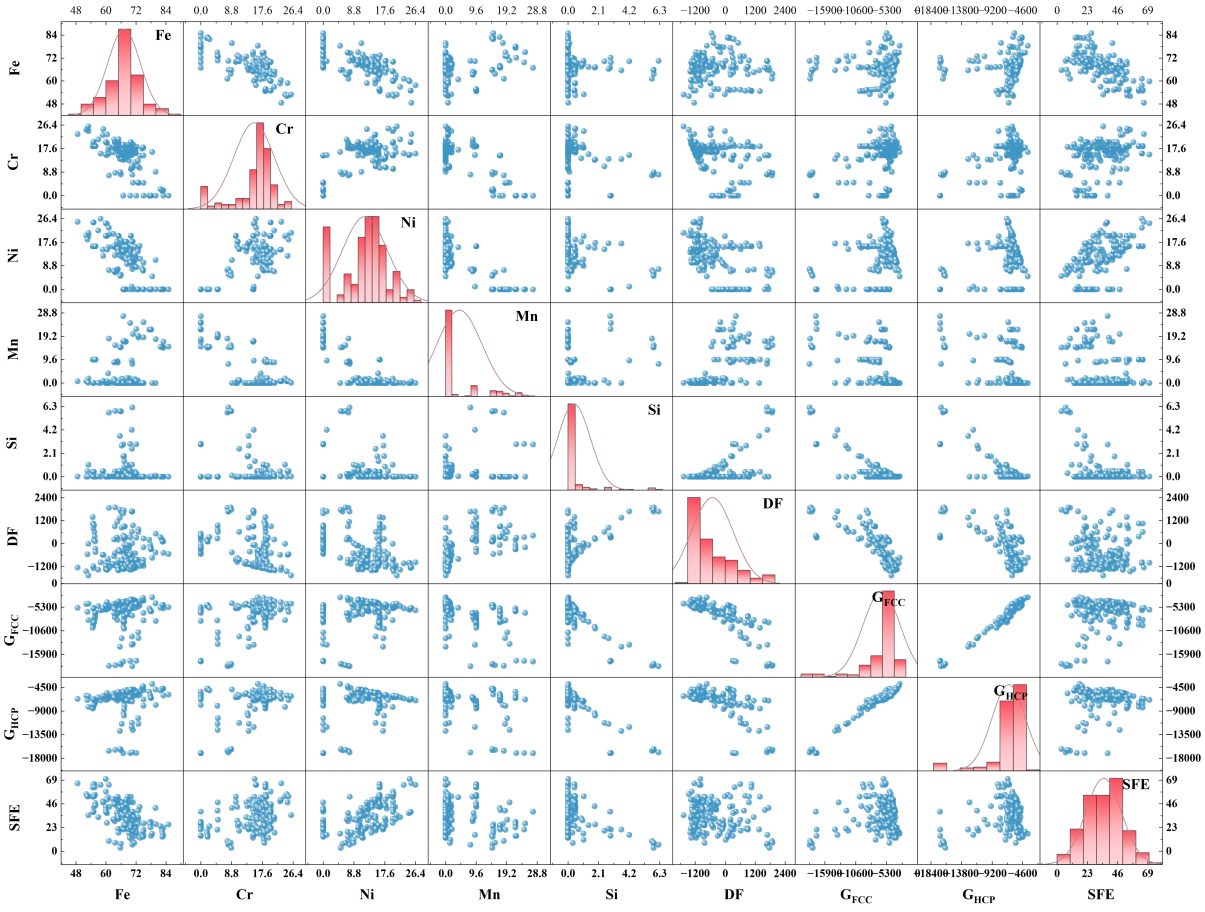

Figure 1. Scatterplot of the distribution matrix of the main features in the dataset.

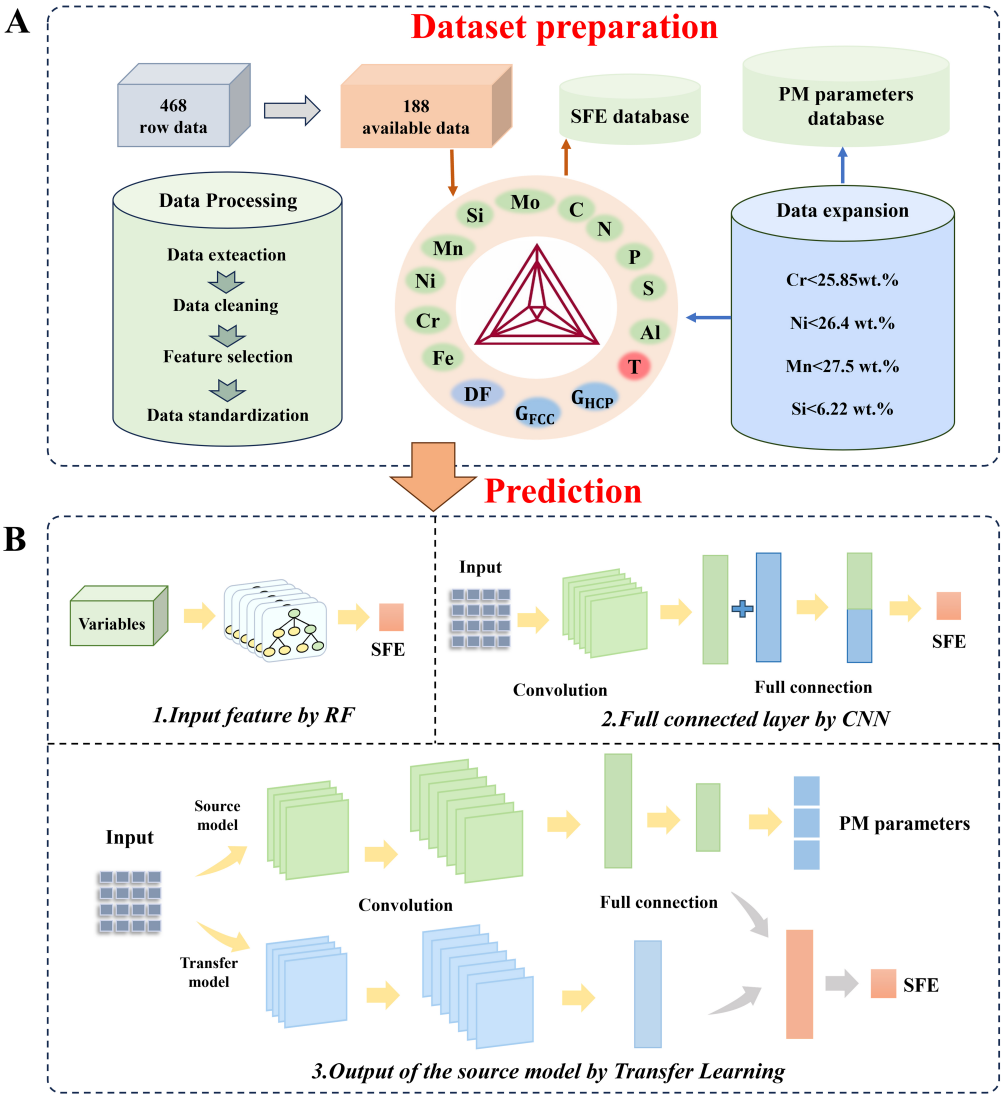

Figure 2. SFE prediction framework. (A) Data processing and dataset expansion; (B) different frameworks for 3 PM parameter introduction methods. SFE: Stacking fault energy; PM: physical metallurgy.

$$z = \frac{x - \mu}{\sigma} \tag{1}$$

where z denotes the normalized value, x is the original value from the dataset, and μ and σ represent the mean and standard deviation of the original values for a certain dimensional feature, respectively.

SFE prediction framework

As previous studies primarily established direct relationships between alloy composition, temperature, and SFE, this study further introduces PM parameters related to the SFE, such as the DF, G_{FCC}, and G_{HCP}. Three approaches for introducing PM parameters in increasing "depth" [Figure 2B] were considered: (1) Direct input: PM parameters, along with alloy composition, were used as input features to predict SFE; (2) Intermediate layer in CNN: PM parameters were introduced into the fully connected layer of the CNN; and (3) Transfer learning: PM parameters were used to train a source model that was then transferred to the SFE prediction model.

When the PM parameters were used as input features, five common ML algorithms were selected to construct the regression prediction models: random forest (RF), gradient boosting regression (GBR), multilayer perceptron (MLP), support vector regression with a radial basis function kernel (SVR), and extreme gradient boosting (XGB). After optimizing each model using grid search, RF was found to perform best for SFE prediction. Various PM-composition combinations were evaluated to assess the influence of PM parameters on SFE prediction accuracy.

In addition to the above approaches, this study explores the introduction of PM parameters into an intermediate layer of the deep learning model. A simple CNN structure was developed, comprising a sequential arrangement of a convolutional layer and a fully connected layer. As shown in Supplementary Figure 2, in this setup, the 11-dimensional constituent features of the alloy samples were finally reshaped into a 4 × 4 matrix (with the alloy compositional features filtered into the matrix by filling them sequentially, and the values of the remaining five elements set to zero) and then fed into a convolution module containing two convolutional layers (4 × 4 × 8 and 4 × 4 × 16). This convolutional module was followed by a fully connected layer with two architectures (64 and eight layers, respectively). At this fully connected layer, PM parameter information was incorporated, and the combined data was fed into the next fully connected layer to predict SFE.

For the transfer learning model, a CNN source model was initially constructed using the aforementioned PM parameter dataset to predict DF, G_{FCC} and G_{HCP} based on the alloy composition. This source model was then used to construct the SFE prediction model. Specifically, the convolutional and fully connected layers of the source model were replicated in the target transfer model, creating a new structure called the transferred feature layer. The parameters of this layer were frozen and did not participate in further training; only the remaining fully connected layers were randomly initialized for model training on SFE prediction.

All data preprocessing and model training were performed using the TensorFlow and Scikit-learn packages. For the CNN model, training was conducted over 500 iterations with mean square error (MSE) as the loss function, a learning rate of 0.1, and the Adam optimizer.

For model performance evaluation, to objectively evaluate the generalization ability of various models and identify the optimal model, the squared correlation coefficient (R^2) and mean absolute error (MAE) were used as evaluation metrics[37,38]. These metrics are expressed as follows:

$$R^2 = \frac{\left(n\sum_{i=1}^{n} f(x_i)y_i - \sum_{i=1}^{n} f(x_i)\sum_{i=1}^{n} y_i\right)^2}{\left(n\sum_{i=1}^{n} f(x_i)^2 - \left(\sum_{i=1}^{n} f(x_i)\right)^2\right)\cdot\left(n\sum_{i=1}^{n} y_i{}^2 - \left(\sum_{i=1}^{n} y_i\right)^2\right)} \quad (2)$$

$$MAE = \frac{1}{n}\sum_{i=1}^{n} |f(x_i) - y_i| \quad (3)$$

where n is the number of samples, and $f(x_i)$ and y_i are the predicted and experimental values of the *i*th sample, respectively.

RESULTS AND DISCUSSION

Feature analysis of composition and PM parameters

In this study, SFE prediction was examined based on the alloy composition and PM parameters. To quantify the relationship and importance of these features in SFE prediction, the Pearson correlation coefficient, Shapley Additive exPlanations (SHAP) value and mean decrease accuracy (MDA) were used[39-41]. The Pearson correlation coefficient was defined as the covariance between two variables divided by the product of their standard deviations. It measures the degree of linear correlation between variables, ranging from -1 to 1, where absolute values closer to 1 indicate a stronger correlation. The SHAP value is a game-theory-based method for interpreting the predictive results of ML models. It helps us to understand how much each feature contributes to the prediction result of the model. MDA assesses the importance of specific features for SFE prediction by disrupting selected compositional or PM parameter features and calculating the resulting decrease in model prediction accuracy.

The Pearson correlation results [Figure 3A] revealed the relationship between alloying elements and SFE. Specifically, Cr, Ni, and Mo exhibited a positive correlation with the SFE values, whereas Mn and Si demonstrated a negative correlation. Notably, this finding partially contrasts with conventional understanding, particularly in austenitic stainless steels, where Cr is generally believed to lower the SFE. In this case, however, the Pearson analysis indicated a positive correlation, potentially influenced by the data on high-Mn steels, as Mn, a strong austenite-stabilizing element, can significantly increase the SFE values. Additionally, correlations among primary alloying elements, such as Cr, Ni, Mn, Si, and PM, are associated with one another, confirming the reasonableness of the selected parameters and underscoring the complexity of their influence on the SFE. The absolute values of the R^2 between each input feature and the SFE were greater than 0 but less than 1, indicating the independent contribution of each feature on SFE and emphasizing the importance of considering the elemental interactions in alloy design.

As shown in Figure 3B, the results of SHAP values demonstrate that both alloy composition and PM parameters contribute to SFE. Specifically, elements such as Ni and Si exhibit significant contributions, highlighting their core position in the process of predicting SFE using the model. Similarly, PM parameters also have an impact on SFE prediction. The SHAP values of DF, G_{FCC}, and G_{HCP} are sequentially ordered, with G_{FCC} being higher than G_{HCP}. This is similar to the results of MDA, as further analyzed in Figure 3C for the predictive significance of each feature: Ni contributed most significantly, with an MDA value exceeding 50%. Previous thermodynamic theoretical studies have shown SFE in FCC alloys to be closely linked with DF and other factors, indicating that PM parameters also contribute to SFE prediction. Among the PM parameters, the MDA values ranked as G_{FCC}, DF, and G_{HCP}, with means G_{FCC} in austenitic steels has significantly higher importance than G_{HCP}.

Reliability analysis of models with PM parameters

In the modeling strategy, where PM parameters are directly introduced as inputs, various common ML algorithms were considered, as outlined previously. In addition, modeling without the PM parameters was evaluated, meaning SFE prediction relied solely on the alloy composition. Figure 4 shows the R^2 and MAE results of different algorithms before and after introducing different PM parameters. All models exhibited noticeable overfitting, with most achieving R^2 values above 95% and MAE below 2 mJ/m^2 for the training set, whereas the R^2 for the testing set ranged from 65%-70% and MAE values were approximately 6 mJ/m^2, indicating suboptimal prediction performance. Specifically, the simple introduction of PM information did not improve the predictive performance of the models, as the R^2 and MAE values were similar between models with and without PM information. Furthermore, no significant difference was observed among different types or combinations of PM information.

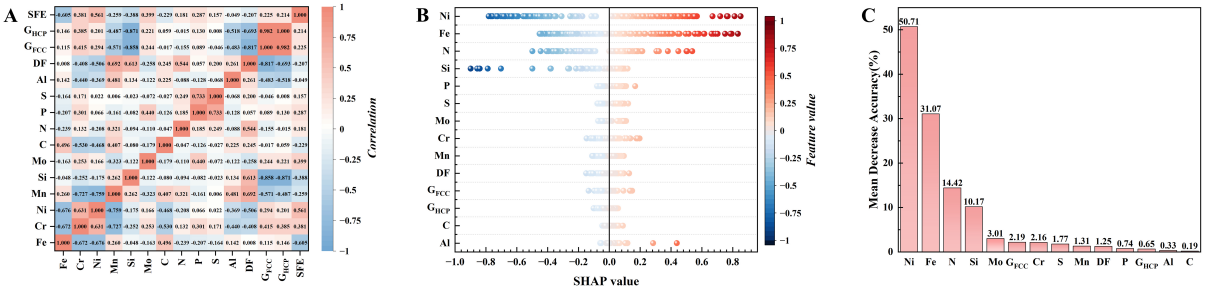

Figure 3. Feature analysis of alloy compositions and PM parameters with respect to SFE. (A) Pearson's correlation coefficient; (B) SHAP values; (C) MDA. PM: Physical metallurgy; SFE: stacking fault energy; SHAP: Shapley Additive exPlanations; MDA: mean decrease accuracy.

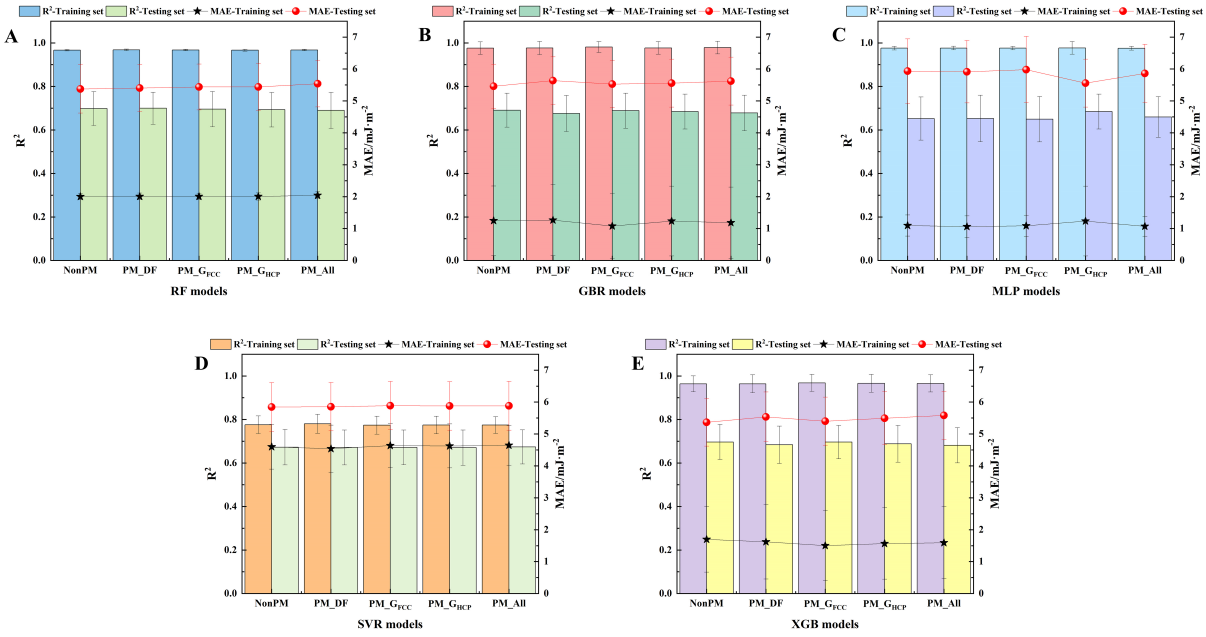

Figure 4. Mean R^2 and MAE results for different PM models using conventional ML algorithms. R^2: The squared correlation coefficient; MAE: mean absolute error; PM: physical metallurgy; ML: machine learning.

This study further investigated the impact of the simple introduction of PM information on model prediction scalability by comparing models without PM information and those introducing all PM parameters (including GBR, MLP, RF, SVR, and XGB) for predicting SFE under single compositional changes. Figure 5 illustrates the trend of the model-predicted SFE variations with changes in the weight percentages (wt.%) of Cr, Ni, Mn, and Si alloying elements. Figure 5A and B shows the average values of SFE for 100 model predictions across five algorithms for Cr content variations (0-25 wt.%). Initially, SFE decreased with increasing Cr content, and then exhibited an upward trend once it decreased to a certain value. Compared to the non-PM control group, the model with the introduction of the PM parameter showed a significant reduction in the range of predicted values and an improvement in the error bars, indicating improved accuracy and stability in SFE predictions. Similarly, as Si increased, SFE decreased, and then increased again before declining [Figure 5G and H]. Guided by PM knowledge, the model with PM parameters effectively avoided negative SFE values. Although the introduction of PM information improved predictive results, its effect varied by element. For instance, the model prediction performance of Ni

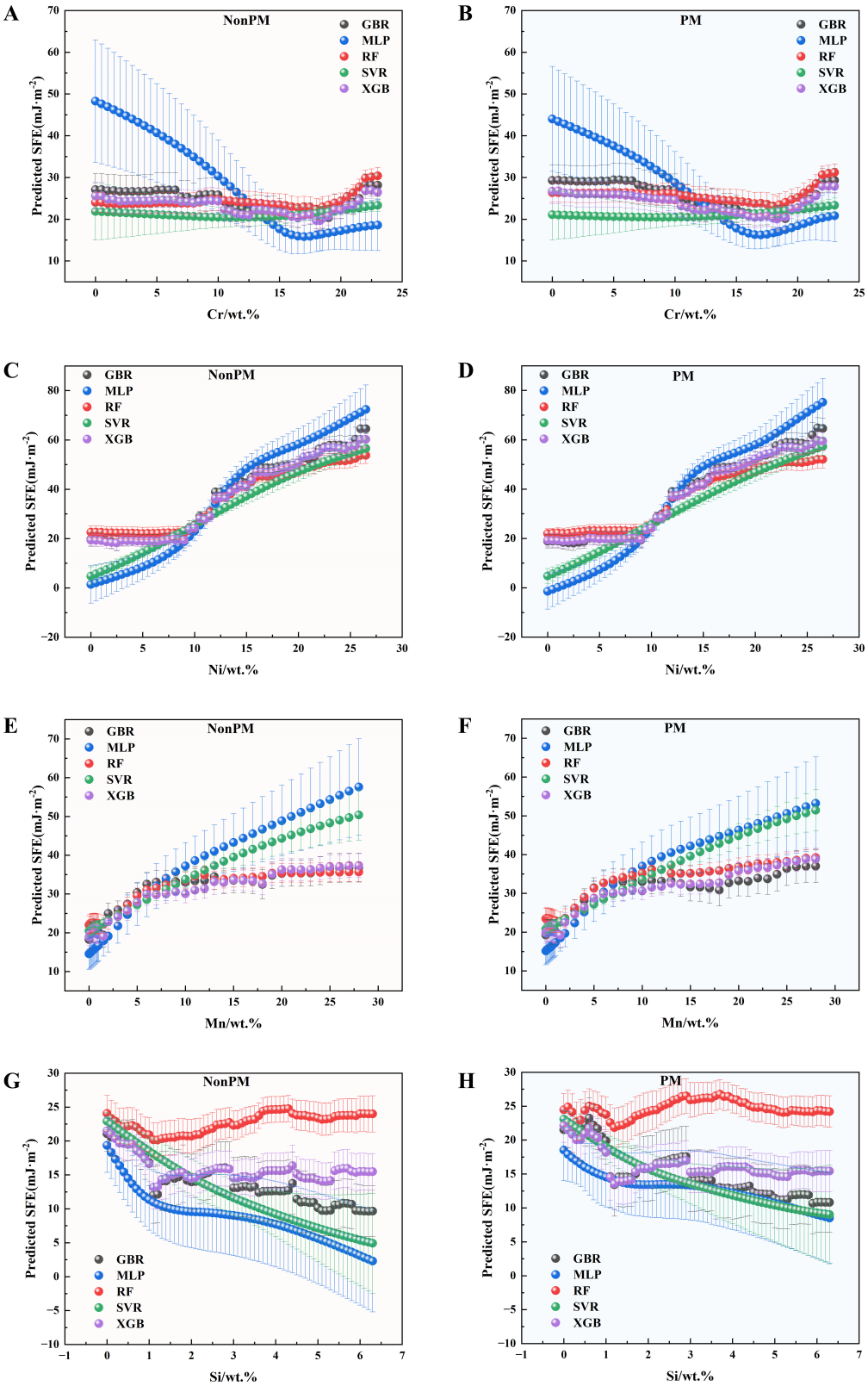

Figure 5. Comparison of SFE trends for component prediction before and after the introduction of PM in different models. (A and B) Cr; (C and D) Ni; (E and F) Mn; (G and H) Si. SFE: Stacking fault energy; PM: physical metallurgy.

[Figure 5C and D] and Mn content [Figure 5E and F] following the introduction of PM parameters was not as notable as it was for Cr and Si. This may be due to the coordinated influence of several elements on SFE, which the model may not capture when only a single element is changed, resulting in predicted values that deviate from actual outcomes. Nevertheless, the introduction of PM parameters can minimize prediction errors and improve the predictive ability of the model to some extent. However, the direct introduction of PM parameters may not be optimal. Further research is needed to better leverage PM information, potentially by introducing PM knowledge to optimize and improve the model for more accurate and reliable SFE predictions.

Impact of PM parameters on the model in different introduction methods

As discussed, introducing PM information as direct input yielded only limited improvement in SFE prediction, even when varying combinations of PM parameters were considered. This section discusses the effects of different PM parameter introduction approaches. Figure 6 shows the model prediction results with different PM information introduced under three frameworks, containing training, testing, and validation sets, including additional austenitic stainless steel samples. The prediction accuracies and errors of the ML models introduced across different PM information for both the training and testing sets were similar for all three frameworks. The main difference was in validation set predictions, highlighting significant differences in model scalability - important for practical applications and alloy design. Before introducing PM parameters, it is notable that, compared to RF algorithms, CNNs show higher flexibility in managing complex and nonlinear data. The convolutional layer of a CNN can automatically extract complex data features, effectively reducing prediction errors in SFE modeling and demonstrating the excellence of CNN modeling.

In the simple PM information introduction approach (e.g., Figure 6A), none of the PM parameter variations improved the generalization ability of the model, with the validation set MAEs consistently exceeding 6 mJ/m^2. By contrast, a deeper PM information introduction, such as the introduction of PM information into the fully connected layer of the CNN [Figure 6B], significantly improved the predictive scalability of the model, reducing the MAE of the validation set to approximately 3 mJ/m^2. Despite the remarkable improvement in prediction ability, the performances of ML models with varying PM information combinations were not significantly different, indicating that the models still had difficulty distinguishing the critical roles of different PM information. By contrast, the transfer learning model with deeply introduced PM information [Figure 6C] achieved the best-extended capacity, and the MAE of the validation set remained consistently below 3 mJ/m^2. Meanwhile, the prediction results from transfer learning models incorporating different combinations of PM information show that building a source model with a single PM information as the target yields the best performance. This approach significantly outperforms models without PM information or those introducing all PM information. In conclusion, when building the source model with DF as the target, the prediction accuracy of the SFE-transferred model was the highest at close to 80%. These results demonstrate that the transfer learning model, with PM information as an intermediate attribute, achieves highly generalized SFE predictions.

This model is not limited to the original alloys in the dataset, but can deeply analyze PM information for both the alloys in the dataset and alloys of similar composition, enabling SFE predictions across a broad range of alloy systems and establishing a foundation for robust predictive scalability. However, this model constructs complex correlations between composition and PM information across diverse alloy composition-PM datasets, an approach absent in previous methods. As shown in Supplementary Figure 3, after expanding the database, the R^2 of the source model increased from 98.5% to 99.8%. Next, we utilized these already-constructed models to further transfer and predict SFE, and verified the generalization ability of the models. Supplementary Figure 3C shows that the prediction accuracy has improved, with the R^2

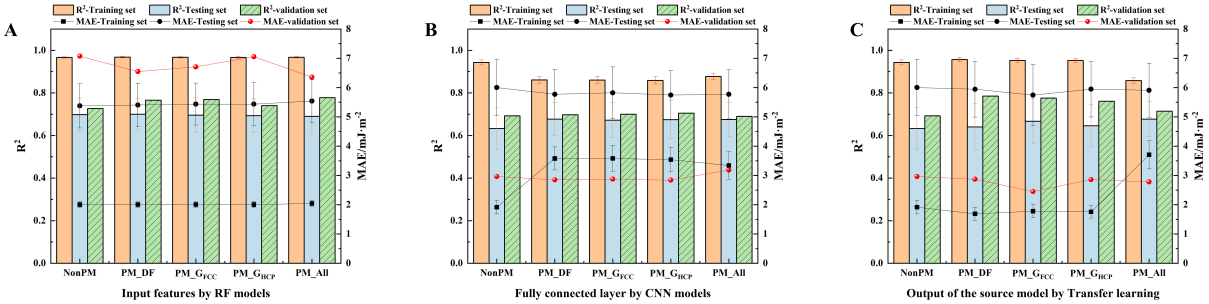

Figure 6. Comparison of model predictions under different introduction methods. (A) Input features by RF models; (B) fully connected layer by CNN models; (C) output of the source model by Transfer learning. RF: Random forest; CNN: convolutional neural network.

increasing from 72.3% to 78.5% while maintaining a low MAE value. This demonstrates that when the source model is trained with PM parameters as the output, generating sufficient virtual samples and fully training the model allows it to capture the underlying relationships between alloy composition and PM parameters. By transferring this complex association to predict SFE compositionally, introducing PM information as an intermediate step significantly enhances the predictive scalability of the model, enabling accurate prediction results even with small sample data, and truly achieving an enhancement in the interpretability of the ML model.

Prediction of SFE based on different PM introduction methods

This study considered three methods for introducing PM parameters into ML modes. As an example of the introduction of DF, Figure 7A shows the prediction results of these models, containing the training set, testing set, and additional sample data of austenitic stainless steel compositions as the validation set. For the training set, all models achieved high accuracy, with $R^2 > 85\%$ and MAE below 4 mJ/m^2, demonstrating the effectiveness of the RF algorithm and CNN in modeling SFE. Meanwhile, the slightly lower accuracy observed in the model incorporating PM parameters at the fully connected layer splicing may be due to the limitation of the small datasets used for deep learning models. For the testing set, the performances of the three models were similar, with prediction accuracies of approximately 70% and errors under 6 mJ/m^2. The validation set, crucial for assessing the generalization ability of the model, revealed more significant differences between strategies. R^2 values for the three models were above 70%, with the TR model having the greatest accuracy (close to 80%). For MAE, the RF model had a significantly higher prediction error (above 6.5 mJ/m^2), whereas the CNN and TR models yielded lower errors (under 3 mJ/m^2), indicating that the transfer-learn strategy exhibited the best prediction performance.

Figure 7B shows the scatter plots of the predictions of the three models for the validation set. The RF model, in which DF was introduced directly as an input, showed the poorest performance, with predictions diverging from actual values. The prediction performance of the CNN model improved significantly, although performance in lower SFE ranges remained suboptimal. In contrast, most of the points predicted by the TR model aligned with the actual values along a line with a slope of 1, achieving the best prediction ability in lower SFE ranges, thereby reducing error and improving accuracy. In addition to DF, similar results were obtained for other PM parameters, indicating that the transfer learning strategy is the most effective approach. The above results indicate that as the "depth" of the PM parameter introduction increases - corresponding to enhanced guidance from PM mechanisms in ML - model generalization ability also improves. The improvement in the generalization ability of the model is still limited under the simple introduction mode of directly taking PM parameter inputs, but improves significantly when PM information is the intermediate (fully connected layer) input to the model. The most substantial

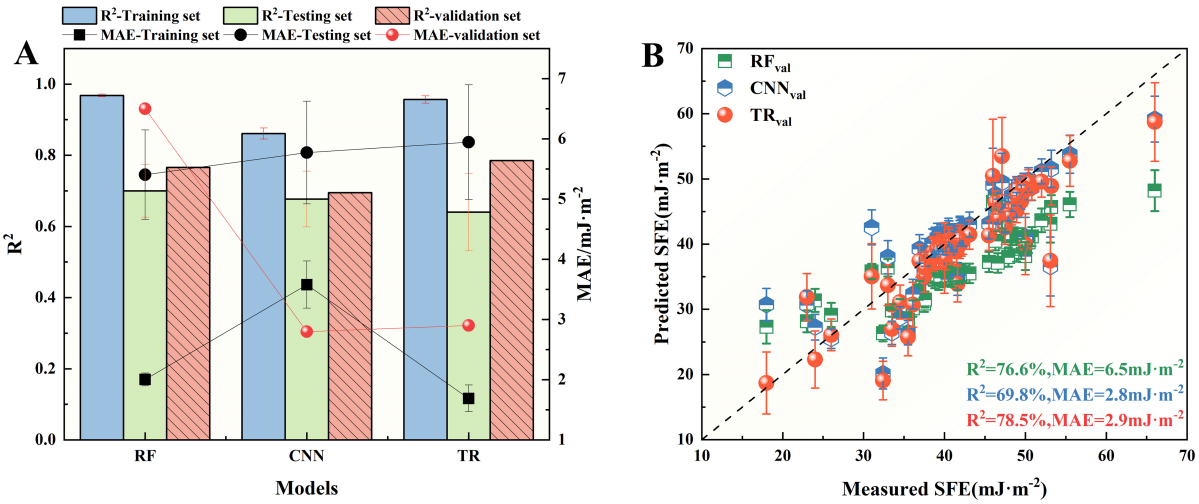

Figure 7. Comparison of model predictions using different methods of introducing DF. (A) R^2 and MAE for training set, testing set, and validation set; (B) distribution of predicted and measured values of SFE for austenitic stainless steels. DF: Driving force; R^2: the squared correlation coefficient; MAE: mean absolute error; SFE: stacking fault energy.

improvement in generalization arises from the transfer learning approach, where a source model with deeply mined PM information is constructed and subsequently transferred to the SFE prediction model. These results provide a reliable strategy for building ML models for SFE prediction, leveraging PM knowledge effectively in small data samples.

CONCLUSIONS

To obtain a generic and accurate prediction of the SFE, this study explored different strategies for introducing PM information into ML models, successfully establishing a framework for efficient prediction using PM information-guided ML. The specific conclusions are as follows:

(1) After comparing various strategies, we found that transfer learning with PM information as an intermediate step yielded the best predictive performance. Specifically, when the RF algorithm is directly applied, the model's MAE reaches as high as 7.1 mJ/m^2. On the other hand, when PM information is simply introduced into the fully connected layer of CNN, the best-achieved R^2 value is only 69.8%. However, when PM information is used as an intermediate step in transfer learning, the model not only achieves a higher R^2 value (up to 78.5%) but also significantly reduces the MAE to 2.9 mJ/m^2, resulting in a substantial improvement in prediction accuracy.

(2) By establishing a component-PM information association as an intermediate section for the composition-SFE relationship, the transfer learning model demonstrated significant improvements in generalization ability. This transfer learning approach allowed the model to identify the key roles of different PM information in SFE prediction, with DF as the source attribute providing the most accurate SFE transfer model, outperforming models that incorporated other PM parameters or their combinations.

DECLARATIONS

Authors' contributions

Made substantial contributions to conception and design of this review, writing and editing: Song L, Wei X, Wang C, Li Y

Made substantial contributions to collation of literature, figure preparation, and writing: Song L, Wei X
Performed data analysis, discussion and review writing: Song L, Wei X
Provided administrative, technical, and material support: Wei X, Li Y

Availability of data and materials

The data supporting the findings of this study are available within the article and its Supplementary Materials. Further data can be obtained from the corresponding authors upon request.

Financial support and sponsorship

The research was financially supported by the National Key Research and Development Program (Grant No. 2022YFB3707501), the Applied Basic Research Program of Liaoning Province (Grant No. 2023JH2/101300147) and the Xingliao Talent Program of Liaoning Province (Grant No. XLYC2203027).

Conflicts of interest

All authors declared that there are no conflicts of interest.

Ethical approval and consent to participate

Not applicable.

Consent for publication

Not applicable.

REFERENCES

1. Wang, Z.; Lu, W.; An, F.; et al. High stress twinning in a compositionally complex steel of very high stacking fault energy. *Nat. Commun.* **2022**, *13*, 3598. DOI PubMed PMC
2. Jeong, J.; Woo, W.; Oh, K.; Kwon, S.; Koo, Y. In situ neutron diffraction study of the microstructure and tensile deformation behavior in Al-added high manganese austenitic steels. *Acta. Mater.* **2012**, *60*, 2290-9. DOI
3. Otte, H. The formation of stacking faults in austenite and its relation to martensite. *Acta. Metall.* **1957**, *5*, 614-27. DOI
4. Wong, S. L.; Madivala, M.; Prahl, U.; Roters, F.; Raabe, D. A crystal plasticity model for twinning- and transformation-induced plasticity. *Acta. Mater.* **2016**, *118*, 140-51. DOI
5. Du, C. Application of Austenitic stainless steel in industry. *Process Equip Piping* 2003;54-7+4. Available from: https://kns.cnki.net/kcms2/article/abstract?v=ufuULlVWCsP94M9oRcpza9IACD4Y12DTBg3Sk2BMrJSDxqS3XZ8gEqE_FwfMraM7fEaSP2vSWE9y-Djer6RVOJ5jasv_m_Zw3uc2nM-iIoDRkDp2sJMSBJWzYnWuUcAuukhmLUi-B6YRzYH_Bd_eqMlHOqmn6UG42Q_jYQJymMXkABxomz6y_f8RqGj9uLvW&uniplatform=NZKPT&language=CHS. (in Chinese) [Last accessed on 4 Jan 2025].
6. Vitos, L.; Nilsson, J.; Johansson, B. Alloying effects on the stacking fault energy in austenitic stainless steels from first-principles theory. *Acta. Mater.* **2006**, *54*, 3821-6. DOI
7. Dong, Z.; Li, W.; Chai, G.; Vitos, L. Strong temperature - dependence of Ni -alloying influence on the stacking fault energy in austenitic stainless steel. *Scr. Mater.* **2020**, *178*, 438-41. DOI
8. Chong, X.; Shang, S. L.; Krajewski, A. M.; et al. Correlation analysis of materials properties by machine learning: illustrated with stacking fault energy from first-principles calculations in dilute fcc-based alloys. *J. Phys. Condens. Matter.* **2021**, *33*, 295702. DOI PubMed
9. Lang, D.; Huang, W. Stacking fault energy in Fe-Mn-C-Si-Cr high manganese steels and experimental investigation. *Foundry Technol* 2021;42:575-8. (in Chinese) Available from: http://211.67.182.139/KCMS/detail/detail.aspx?filename=ZZJS202107006&dbcode=CJFD&dbname=DKFX2021. [Last accessed on 4 Jan 2025].
10. Lee, S. J.; Jung, Y. S.; Baik, S. I.; et al. The effect of nitrogen on the stacking fault energy in Fe–15Mn–2Cr–0.6C–*x*N twinning-induced plasticity steels. *ScrMater* **2014**, *92*, 23-6. DOI
11. Whelan, M. J. Dislocation interactions in face-centred cubic metals, with particular reference to stainless steel. *Proc. R. Soc. Lond. A.* **1959**, *249*, 114-37. DOI
12. Abrassart, F. Stress-induced γ→α martensitic transformation in two carbon stainless steels. Application to trip steels. *Metall. Trans.* **1973**, *4*, 2205-16. DOI

13. Yonezawa, T.; Suzuki, K.; Ooki, S.; Hashimoto, A. The effect of chemical composition and heat treatment conditions on stacking fault energy for Fe-Cr-Ni austenitic stainless steel. *Metall. Mater. Trans. A.* **2013**, *44*, 5884-96. DOI
14. Reed, R. P.; Schramm, R. E. Relationship between stacking-fault energy and x-ray measurements of stacking-fault probability and microstrain. *J. Appl. Phys.* **1974**, *45*, 4705-11. DOI
15. Schramm, R. E.; Reed, R. P. Stacking fault energies of seven commercial austenitic stainless steels. *Metall. Trans. A.* **1975**, *6*, 1345-51. DOI
16. Rhodes, C. G.; Thompson, A. W. The composition dependence of stacking fault energy in austenitic stainless steels. *Metall. Trans. A.* **1977**, *8*, 1901-6. DOI
17. Ojima, M.; Adachi, Y.; Tomota, Y.; Ikeda, K.; Kamiyama, T.; Katada, Y. Work hardening mechanism in high nitrogen austenitic steel studied by in situ neutron diffraction and in situ electron backscattering diffraction. *Mater. Sci. Eng. A.* **2009**, *527*, 16-24. DOI
18. de Bellefon G, van Duysen J, Sridharan K. Composition-dependence of stacking fault energy in austenitic stainless steels through linear regression with random intercepts. *J. Nucl. Mater.* **2017**, *492*, 227-30. DOI
19. Olson, G. B.; Cohen, M. A general mechanism of martensitic nucleation: Part I. General concepts and the FCC → HCP transformation. *Metall. Trans. A.* **1976**, *7*, 1897-904. DOI
20. Yang, W. S.; Wan, C. M. The influence of aluminium content to the stacking fault energy in Fe-Mn-Al-C alloy system. *J. Mater. Sci.* **1990**, *25*, 1821-3. DOI
21. Allain, S.; Chateau, J.; Bouaziz, O.; Migot, S.; Guelton, N. Correlations between the calculated stacking fault energy and the plasticity mechanisms in Fe–Mn–C alloys. *Mater. Sci. Eng. A.* **2004**, *387-9*, 158-62. DOI
22. Xiong, R.; Peng, H.; Si, H.; Zhang, W.; Wen, Y. Thermodynamic calculation of stacking fault energy of the Fe–Mn–Si–C high manganese steels. *Mater. Sci. Eng. A.* **2014**, *598*, 376-86. DOI
23. Masumura, T.; Nakada, N.; Tsuchiyama, T.; Takaki, S.; Koyano, T.; Adachi, K. The difference in thermal and mechanical stabilities of austenite between carbon- and nitrogen-added metastable austenitic stainless steels. *Acta. Mater.* **2015**, *84*, 330-8. DOI
24. Aristeidakis, J. S.; Haidemenopoulos, G. N. Composition and processing design of medium-Mn steels based on CALPHAD, SFE modeling, and genetic optimization. *Acta. Mater.* **2020**, *193*, 291-310. DOI
25. Hohenberg, P.; Kohn, W. Inhomogeneous electron gas. *Phys. Rev.* **1964**, *136*, B864-71. DOI
26. Geng, X.; Wang, F.; Wu, H.; et al. Data-driven and artificial intelligence accelerated steel material research and intelligent manufacturing technology. *Mater. Genome. Eng. Adv.* **2023**, *1*, e10. DOI
27. Zhu, L.; Luo, Q.; Chen, Q.; et al. Prediction of ultimate tensile strength of Al-Si alloys based on multimodal fusion learning. *Mater. Genome. Eng. Adv.* **2024**, *2*, e26. DOI
28. Chaudhary, N.; Abu-Odeh, A.; Karaman, I.; Arróyave, R. A data-driven machine learning approach to predicting stacking faulting energy in austenitic steels. *J. Mater. Sci.* **2017**, *52*, 11048-76. DOI
29. Khan, T. Z.; Kirk, T.; Vazquez, G.; et al. Towards stacking fault energy engineering in FCC high entropy alloys. *Acta. Mater.* **2022**, *224*, 117472. DOI
30. Li, H.; Wang, X.; Song, Y.; Li, Y.; Li, X.; Ji, Y. Physical metallurgy guided machine learning to predict hot deformation mechanism of stainless steel. *Mater. Today. Commun.* **2023**, *36*, 106779. DOI
31. Shen, C.; Wang, C.; Rivera-díaz-del-castillo, P. E.; et al. Discovery of marageing steels: machine learning vs. physical metallurgical modelling. *J. Mater. Sci. Technol.* **2021**, *87*, 258-68. DOI
32. Cui, C.; Cao, G.; Li, X.; Gao, Z.; Liu, J.; Liu, Z. A strategy combining machine learning and physical metallurgical principles to predict mechanical properties for hot rolled Ti micro-alloyed steels. *J. Mater. Process. Technol.* **2023**, *311*, 117810. DOI
33. Shen, C.; Wang, C.; Wei, X.; Li, Y.; van, Z. S.; Xu, W. Physical metallurgy-guided machine learning and artificial intelligent design of ultrahigh-strength stainless steel. *Acta. Mater.* **2019**, *179*, 201-14. DOI
34. Basha, S. S.; Dubey, S. R.; Pulabaigari, V.; Mukherjee, S. Impact of fully connected layers on performance of convolutional neural networks for image classification. *Neurocomputing* **2020**, *378*, 112-9. DOI
35. Wei, X.; van, Z. S.; Jia, Z.; Wang, C.; Xu, W. On the use of transfer modeling to design new steels with excellent rotating bending fatigue resistance even in the case of very small calibration datasets. *Acta. Mater.* **2022**, *235*, 118103. DOI
36. Jain, A.; Nandakumar, K.; Ross, A. Score normalization in multimodal biometric systems. *Pattern. Recognit.* **2005**, *38*, 2270-85. DOI
37. Liu, X.; Xu, P.; Zhao, J.; Lu, W.; Li, M.; Wang, G. Material machine learning for alloys: applications, challenges and perspectives. *J. Alloys. Compd.* **2022**, *921*, 165984. DOI
38. Ilyas, N.; Shahzad, A.; Kim, K. Convolutional-neural network-based image crowd counting: review, categorization, analysis, and performance evaluation. *Sensors* **2019**, *20*, 43. DOI PubMed PMC
39. Kim, Y.; Kim, T.; Ergün, T. The instability of the Pearson correlation coefficient in the presence of coincidental outliers. *Financ. Res. Lett.* **2015**, *13*, 243-57. DOI
40. Jeon, J.; Seo, N.; Son, S. B.; Lee, S.; Jung, M. Application of machine learning algorithms and SHAP for prediction and feature analysis of tempered martensite hardness in low-alloy steels. *Metals* **2021**, *11*, 1159. DOI
41. Wei, J.; Chu, X.; Sun, X.; et al. Machine learning in materials science. *InfoMat* **2019**, *1*, 338-58. DOI